Modulating Density of Catalytic Sites in Multiple-Component Covalent Organic Frameworks for Electrocatalytic Carbon Dioxide Reduction

Minghao Liu,[†, ‡, &] *Xingyue Zhao,*[† &] *Shuai Yang,*[† &] *Xiubei Yang,*[†, §] *Xuewen Li,*[†, §] *Jun He,**[‡, ƒ] *George Zheng Chen,*[#] *Qing Xu**[†, §] *and Gaofeng Zeng**[†, §]

[†] CAS Key Laboratory of Low-Carbon Conversion Science and Engineering, Shanghai Advanced Research Institute, Chinese Academy of Sciences, Shanghai 201210, China

[‡] Department of Chemical and Environmental Engineering, University of Nottingham Ningbo China, Ningbo 315199, China

[§] School of Chemical Engineering, University of Chinese Academy of Sciences, Beijing 100049, China

[ƒ] Nottingham Ningbo China Beacon of Excellence Research and Innovation Institute, Ningbo 315100, China

[#] Department of Chemical and Environmental Engineering, University of Nottingham, Nottingham NG7 2RD, UK

KEYWORDS: Covalent organic frameworks, carbon dioxide reduction reaction, structure−property correlation, phthalocyanine, alternate structure

ABSTRACT: It is generally assumed that the more metal atoms in covalent organic frameworks (COFs) contribute to higher activity towards electrocatalytic carbon dioxide reduction (CO_2RR), and hindered us to explore the correlation between the density of catalytic sites and catalytic performances. Herein, we have constructed quantitative density of catalytic sites in multiple-COFs for CO_2RR, in which the contents of phthalocyanines (H_2Pc) and Ni-phthalocyanines (NiPc) units were preciously controlled. With the molar ratio of 1/1 for H_2Pc and NiPc units in the COFs, the catalyst achieved highest selectivity with the CO Faradaic efficiency (FE_{CO}) of 95.37% and activity with the turnover frequency (TOF) of 4713.53 h^{-1}. In the multiple H_2Pc/NiPc-COFs, the electron-donating features of H_2Pc units provide electrons transport to NiPc centers and thus improved the binding ability of CO_2 and intermediates on the NiPc units. The theoretical calculation further confirmed that the H_2Pc unites donated their electrons to NiPc units in the frameworks, and enhance the electron density of Ni sites and improved the binding ability with Lewis acidic CO_2 molecules, thereby boosting the CO_2RR performance. This study provides us a new insight into design highly active catalysts in electrocatalytic systems.

Introduction

The electrocatalytic carbon dioxide reduction (CO_2RR) into value-added fuels and chemical feedstock is a prospective technology to achieve carbon neutralization.[1-5] However, there are still several problems in the electrocatalysis process for CO_2RR, including the large energy which activated the inert CO_2, the multielectron transfer processes and the low availability of

catalytic sites led the poor product selectivity and the competitive hydrogen evolution reaction (HER).[6-14] The catalytic properties not only depend on the kinds of metal centres and their coordination environments, but also rely on the density of the metal atoms.[15-18] However, how to preciously control the contents of metal sites is hardly achieved in the carbon-based catalysts.[19-22]

Covalent organic frameworks (COFs), as one kind of porous organic materials, have attracted considerable attention for various applications such as gas/molecular absorption, photo- / electro-catalysis, lithium- batteries and energy storge systems.[23-34] With using various functional units, COFs have been utilized in oxygen reduction reaction, oxygen evolution reaction (OER), hydrogen evolution reaction (HER), H_2O_2 synthesis.[35-39] Among catalytic COFs, Metal-Por and Metal-Pc units have been widely employed to catalyze CO_2RR since 2015.[40] Till now, the different metal species, topologies, linkers and linkages have been adopted to improve the activity and selectivity.[41-46] However, modulating the metal density in COFs to tune the catalytic behaviour for CO_2RR is ignored, because it is generally assumed that the more metals results in better catalytic activity. Thus, the correlation between the density of metal atoms and catalytic performances have not been explored.

Herein, we demonstrated for the first time the multiple-component synthesis strategy to construct the controllable metal density in the skeletons of COFs. This strategy enables a quantitative correlation between the metal density and catalytic performance and shows us how to optimize the activity and selectivity. To exclude the effects of linkers and linkages in the COFs for CO_2RR, all the H_2Pc and NiPc are confused with benzene units directly, without any other building units. The alternate H_2Pc in the skeletons enables to promote the electron transfer to the NiPc units. The optimized COF showed high activity and selectivity, with TOFs of 4909.87 h^{-1} at –1.0 V and FE_{CO}

of 95.37% at –0.8 V, respectively. This opens a way to guide the predesign electrocatalysts with higher atomic utilization efficiency.

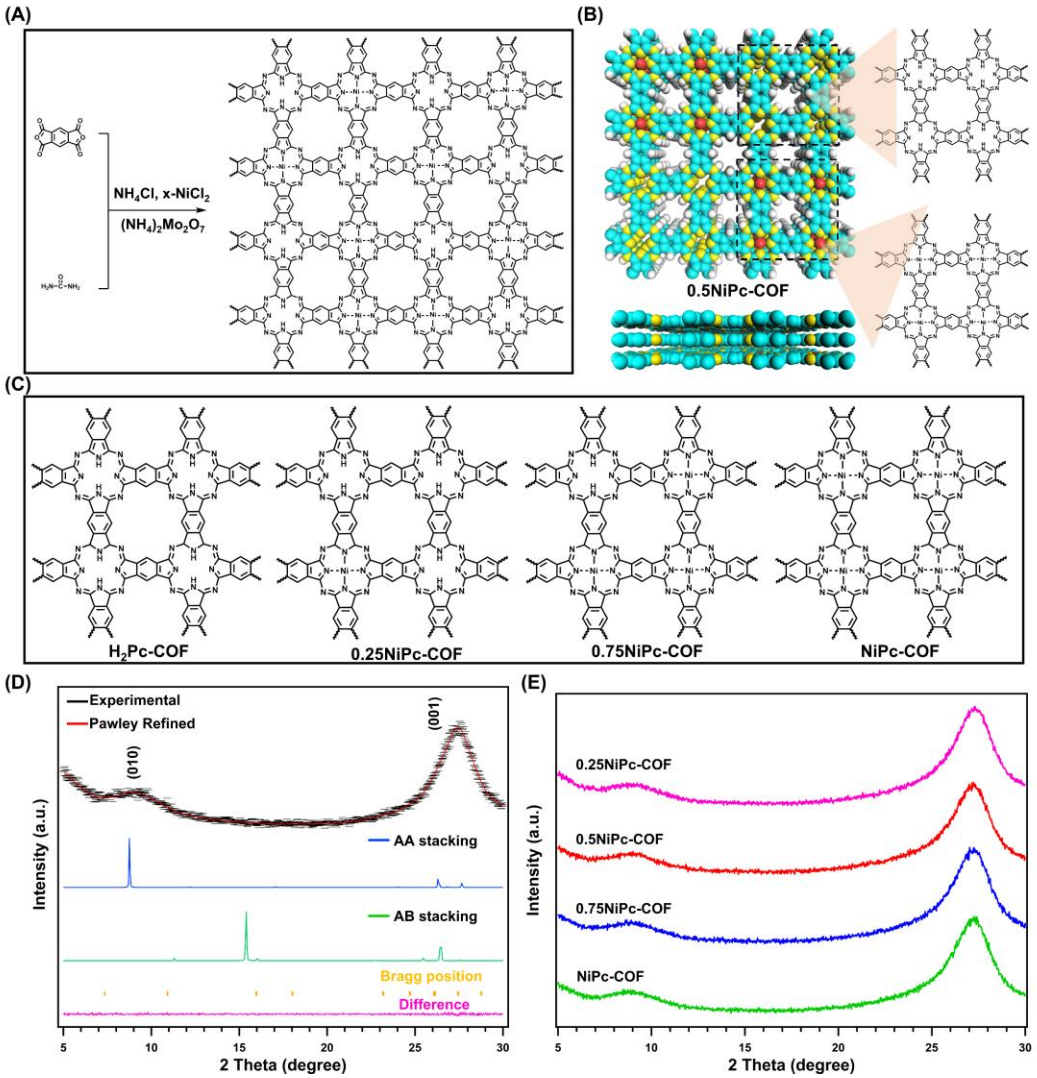

Figure 1. (A) Synthesis of XNiPc-COFs (H_2Pc-COF, 0.25NiPc-COF, 0.5NiPc-COF, 0.75NiPc-COF and NiPc-COF) from PADA, urea, NH_4Cl, $NiCl_3$ and $(NH_4)_2Mo_2O_7$, respectively, with (B) top view and side view of the slipped AA stacking structure (C-cyan, N-yellow, Ni-red) for 0.75NiPc-COFs. (C) The structures of H_2Pc-COF, 0.25NiPc-COF, 0.75NiPc-COF and NiPc-COF. (D) PXRD profiles of H_2Pc-COF of the experimentally observed (black), Pawley refined

(red) and their difference (pink), simulated using the AA (blue) and staggered AB (green) stacking modes. (E) PXRD profiles of 0.25NiPc-COF (pink), 0.5NiPc-COF (red), 0.75NiPc-COF (blue) and NiPc-COF (green).

Experimental Methods

The metal-free COF (H_2Pc-COF) was synthesized from pyromellitic dianhydride (PMDA) (1.86 mmol), urea (40.10 mmol), $(NH_4)_2M_2O_7$ (1.17 mmol) and NH_4Cl (5.00 mmol) at 180 °C for 3 hours by solid-phase synthesis according to previous reports.[47] To achieve different contents of Ni in the COFs, 0.21 mmol, 0.42 mmol, and 0.63 mmol $NiCl_2$ were added in the mixtures to yield XNiPc-COF, X = 0.25, 0.5, and 0.75 (0.25NiPc-COF, 0.5NiPc-COF, 0.75NiPc-COF) respectively (Figure 1A-C). With additional of 0.84 mmol $NiCl_2$ in the mixture, the NiPc-COF was synthesized. The weight contents of Ni in the COFs revealed by ICP measurement were 3.03%, 5.75%, 7.81% and 9.57% for 0.25NiPc-COF, 0.5NiPc-COF, 0.75NiPc-COF and NiPc-COF, which were close to theoretical values (3.22%, 6.06%, 8.57% and 10.81%, respectively.).

Results and discussion

The structures of as-synthesized COFs were investigated using Fourier transform infrared (FT-IR) spectroscopy. It demonstrated that the obvious peak at about 1625 cm^{-1} was assigned to C=N bonds for H_2Pc-COF.[48] And the peaks at nearly 750 cm^{-1} originated from the Ni-N bonds of XNiPc-COFs. These results suggested that the COFs have been successfully synthesized (Figure S1).

Powder X-ray diffraction (PXRD) measurement was conducted to confirm the crystallinities of these COFs. Exactly, the peaks at 8.36 and 27.5 ° were clearly observed, which were from (010)

and (001) facets of H_2Pc-COF (Figure 1D). Additionally, the theoretical structure was the simulated by the Materials Studio package. The simulated PXRD patterns are in good agreement with experimental results (R_{wp} of 3.23% and R_p of 2.96%, respectively). Furthermore, the AA stacking models of H_2Pc-COF matched well with the experimental results and adopted the *P4M* space group, following the cell parameters of a = 10.70 Å, b = 10.70 Å, c = 3.45 Å, $\alpha = \beta = \gamma = 90^o$ (Figure S2 and Tables S1-S2). With immobilizing Ni atoms in the COFs (0.25NiPc-COF, 0.5NiPc-COF, 0.75NiPc-COF and NiPc-COF), the obvious peaks from (010) and (001) were confirmed without position shift, confirming the crystal structures were as same as that of metal-free COFs (Figure 1E and Figures S3-S6).

The porous structures of five as-synthesized COFs were confirmed using nitrogen adsorption isotherm at 77 K. These H_2Pc-COF and XNiPc-COF demonstrated the curves with IV-types (Figure S7). Correspondingly, the Brunauer-Emmett-Teller (BET) surface areas for H_2Pc-COF, 0.25NiPc-COF, 0.5NiPc-COF, 0.75NiPc-COF and NiPc-COF were 24.32, 28.98, 28.11, 46.76 and 88.66 $m^2\ g^{-1}$, with pore volumes of 0.11, 0.09, 0.08, 0.15 and 0.21 $cm^3\ g^{-1}$, respectively. The low permanent porosity could be attributed to the random displacement of the 2D layers to some extent.[49]

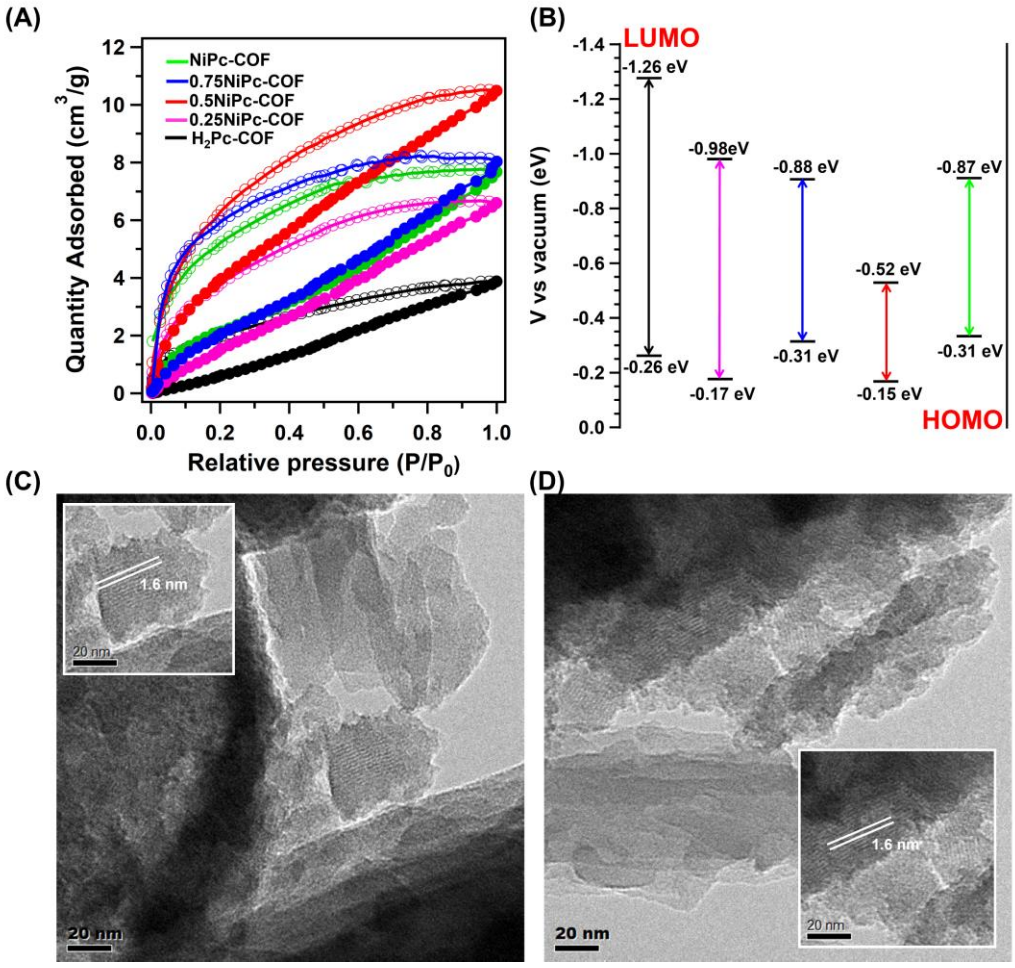

Figure 2. (A) The CO_2 absorption curves at 298 K and (B) the energy gap (HOMO and LUMO) of H_2Pc-COF (black), 0.25NiPc-COF (pink), 0.5NiPc-COF (red), 0.75NiPc-COF (blue) and NiPc-COF (green). The TEM images of (C) H_2Pc-COF and (D) NiPc-COF.

Considering the important role of CO_2 absorption ability for CO_2RR, the CO_2 sorption behaviour at 298 K was investigated. The CO_2 physical-sorption capacity depends on the surface areas and the chemical-sorption rely on the numbers of binding sites. With increasing the contents of Ni, the larger sorption loops suggested the higher binding ability of CO_2. The H_2Pc-COF, 0.25NiPc-COF, 0.5NiPc-COF, 0.75NiPc-COF and NiPc-COF had moderate CO_2 uptake capacities of 3.88, 6.60, 10.51, 8.31 and 8.04 $cm^3\ g^{-1}$ at 1.0 bar, respectively (Figures 2A). With introducing the Ni sites in

the COFs, the CO_2 uptake capacity were obviously improved, which is benefit for improving catalytic activity of CO_2RR.

To explore the properties of prepared XNiPc-COFs, the ultraviolet–visible (UV-Vis) spectroscopy was adopted (Figure S8). Specifically, the Tauc plots demonstrated that the H_2Pc-COF, 0.25NiPc-COF, 0.5NiPc-COF, 0.75NiPc-COF and NiPc-COF had band gaps of 0.39, 0.32, 0.18, 0.28 and 0.27 eV, respectively, indicating that 0.75NiPc-COF favoured the electron transfer in the process of electrocatalysis CO_2RR (Figure 2B).[50] Then, the highest occupied molecular orbital (HOMO) and lowest unoccupied molecular orbital (LUMO) were identified using the Mott-Schottky method. The HOMO positions for H_2Pc-COF, 0.25NiPc-COF, 0.5NiPc-COF, 0.75NiPc-COF and NiPc-COF were -0.26, -0.17, -0.15, -0.31 and -0.31 eV, respectively, indicating that 0.75NiPc possessed better reduction performance than that of other COFs (Figure 2B and Figure S9). We also tested the conductivity of NiPc-COF and 0.5NiPc-COF by the four-probe method at 298 K. The electrical conductivity for NiPc-COF was determined to be 2.8×10^{-5} S cm^{-1}, which is closed to the 0.5NiPc-COF (2.5×10^{-5} S cm^{-1}) (Figure S10).

The field-emission scanning electron microscopy (FE-SEM) demonstrated that H_2Pc-COF was in rodlike shape as the same the other four synthesized XNiPc-COFs (Figures S11-S15). In addition, the transmission electron microscopy (TEM) and high-resolution (HR-TEM) characterization of H_2Pc-COF exhibited the interlayer distance of 1.6 nm, confirming the crystal structure (Figure 2C). With the addition of nickel, NiPc-COF also exhibited a good crystallinity with the similar morphologies (Figure 2D and Figures S16-S18). These results suggested that there is no significant morphological difference with the introduction of nickel, further indicating that the structure is well preserved. Furthermore, the energy dispersive X-ray spectroscopy (EDX)

mapping images revealed that C, N and Ni are uniformly distributed over the COFs (Figures S19-S23).

Then, the chemical and thermal stability of XNiPc-COFs were studied. The XNiPc-COFs were immersed into harsh conditions, including HCl (1.0 M), NaOH (1.0 M) and $KHCO_3$ (0.5 M) for one week. The mass and crystallinity showed no obvious change from PXRD patterns, suggesting the well retained crystal structure (Figure S24). We have also used the thermogravimetric analysis (TGA) measurement to investigate the thermal stability, confirming that no obvious change up to 300 °C under N_2 of these XNiPc-COFs (Figure S25). Then, we also tested the thermal stability of these COFs under air atmosphere by the TGA measurement. The TGA curves demonstrated that the H_2Pc-COF, 0.25NiPc-COF, 0.5NiPc-COF, 0.75NiPc-COF and NiPc-COF left 29%, 27%, 25%, 22% and 20% after 550 °C under air (Figure S26).

Moreover, the hydrophobic characteristics of these COFs were conducted by the contact angle measurements with water (Figure S27). The contact angle of the H_2Pc-COF was 95.37±4.3°, while the 0.25NiPc-COF, 0.5NiPc-COF, 0.75NiPc-COF and NiPc-COF were 125.69±5.8°, 126.15±3.1°, 126.9±4.6° and 127.53±3.4°, respectively. The H_2Pc-COF demonstrated a lower water contact angle compared with that of NiPc-contained COFs, suggesting that water could be accessible to the surface, further facilitating proton transfer and hindering CO_2RR.[51]

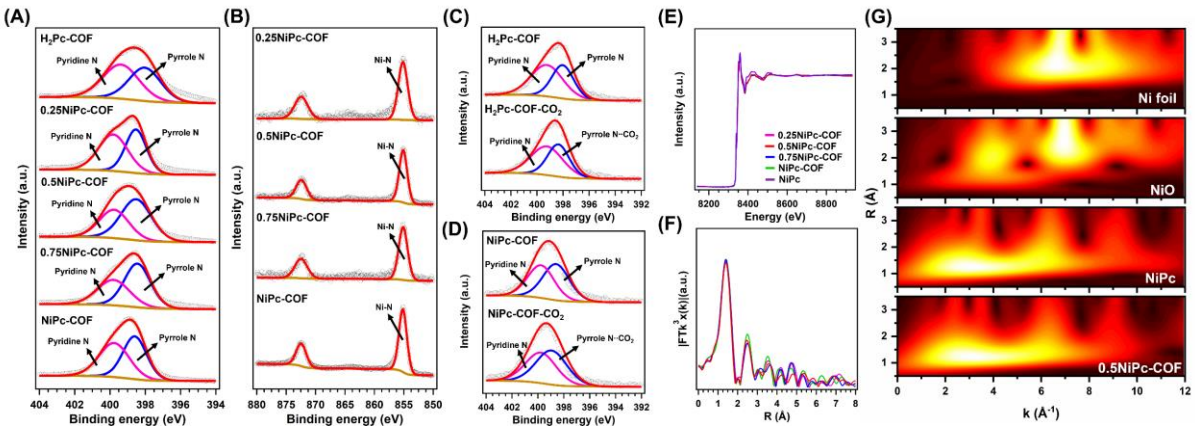

Figure 3. (A) The XPS spectra of N 1s and (B) Ni 2p for H_2Pc-COF, 0.25NiPc-COF, 0.5NiPc-COF, 0.75NiPc-COF and NiPc-COF. The XPS spectra of N 1s of (C) H_2Pc-COF and (D) NiPc-COF in-situ the CO_2 adsorption under the moderate pressure. (E) the XANES spectra and (F) the K-edge k^3-weighted Fourier transform spectra from EXAFS for Ni of NiPc (purple curve), 0.25NiPc-COF (pink curve), 0.5NiPc-COF (red curve), 0.75NiPc-COF (blue curve) and NiPc-COF (green curve). (G) The WT-EXAFS of the Ni foil, NiPc and 0.5NiPc-COF.

X-ray photoelectron spectroscopy (XPS) was performed to explore the chemical structures and electron states of these COFs. Correspondingly, the high-resolution N 1s spectra of these H_2Pc-COF demonstrated peaks at 398.02 and 399.37 eV for pyrrole N and pyridine N, respectively. After the introduction of nickel, the N 1s spectra of 0.25NiPc-COF, 0.5NiPc-COF, 0.75NiPc-COF showed a positive shift compared with that of the H_2Pc-COF. Specifically, the pyridine N had a positive shift of about 0.3 eV, while the pyrrole N had no change, suggesting the successful coordination between pyridine N and nickel (Figure 3A). Additionally, the high-resolution Ni 2p spectra of 0.25NiPc-COF, 0.5NiPc-COF, 0.75NiPc-COF and NiPc-COF exhibited two distinct peaks at about 855.12 eV ($2p_{3/2}$) and 872.43 eV ($2p_{1/2}$), attributing to the Ni-N coordination (Figure 3B). Furthermore, the binding energy of Ni-N was slightly negative shift with 0.13 eV for

0.25NiPc-COF, 0.5NiPc-COF and 0.75NiPc-COF compared with that of NiPc-COF due to the H_2Pc units adjusted the local electron density of the active Ni-N sites, which benefits the adsorption of reactant molecules and transfers more electrons to the reaction.[58]

To further study the CO_2 adsorption sites in these COFs, the in-situ XPS was measured under the ambient pressure with 0.1 mbar CO_2 atmosphere. Specifically, the high-resolution N 1s spectra of H_2Pc-COF demonstrated that the absence of shift for pyridine N, while the pyrrole N showed a positive shift with the value of 0.3 eV (Figure 3C). With immobilizing Ni atoms, the high-resolution N 1s spectra of NiPc-COF also exhibited the same trends with that of the H_2Pc-COF. In addition, the high-resolution N 1s spectra of other XNiPc-COFs also exhibited a positive shift of the pyridine N (Figure 3D and Figure S28). These results suggested that the pyrrole N as 'CO_2 traps' in the vacancies of the structure can adsorb CO_2 which can accelerate the electron supply and transport, further boosting the CO_2RR.[52]

The X-ray absorption fine structure (XAFS) measurements were adopted to further confirm the electronic and atomic states of Ni in 0.25NiPc-COF, 0.5NiPc-COF, 0.75NiPc-COF and NiPc-COF. As shown in Figure 3E, the location of Ni absorption near-edge of 0.25NiPc-COF (pink curve), 0.5NiPc-COF (green curve), 0.75NiPc-COF (blue curve) and NiPc-COF (red curve) exhibited different structures from Ni foil and NiO (Figure S29), but they approached simple substances (NiPc) (purple curve). Furthermore, the peak positions of Ni in R-space about 0.25NiPc-COF, 0.5NiPc-COF, 0.75NiPc-COF and NiPc-COF were 4.9±0.7, 4.6±1.2, 4.8±1.5 and 4.7±1.4 Å, which was close to that of NiPc coordination (Figure 3F). In addition, the EXAFS fitting results demonstrated the existence of $Ni-N_4$ coordination for Ni atom in 0.25NiPc-COF, 0.5NiPc-COF, 0.75NiPc-COF and NiPc-COF (Figure S30 and Table S3). Additionally, to further confirm the combination of Ni, the wavelet transform (WT) of the Ni L^3-edge EXAFS oscillations

was conducted (Figure 3G). 0.5NiPc-COF and NiPc exhibited an intensity maximum at 2.3 $Å^{-1}$ (Ni-N), while only a predominate intensity maximum at higher k-space (6.2 $Å^{-1}$) for Ni foil and 6.5 $Å^{-1}$ for NiO, suggesting the absence of the Ni-Ni or Ni-O metallic coordination, further proving that no metal nanoparticles are present in four COFs.

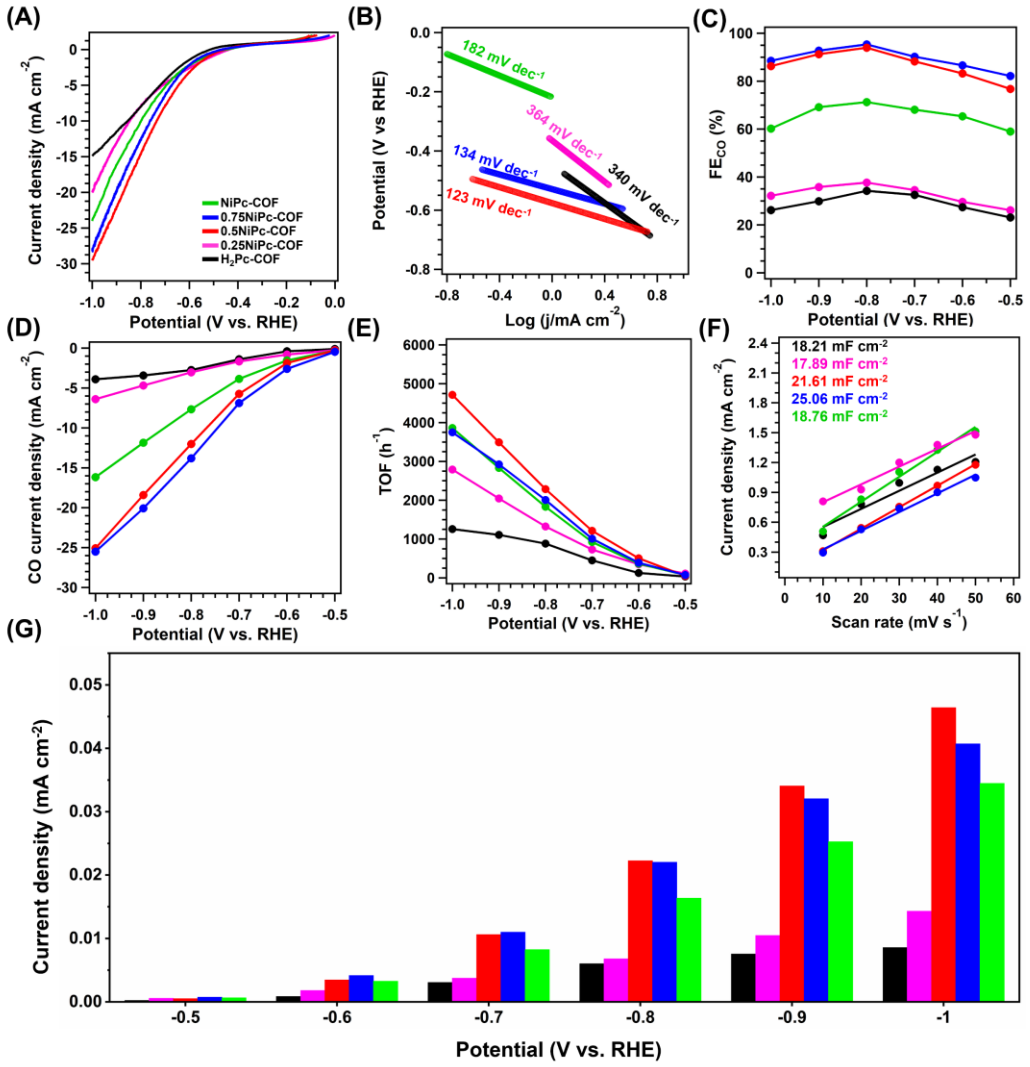

Figure 4. (A) LSV curves, (B) Tafel slopes, (C) CO faradaic efficiency, (D) the partial CO current density, (E) the corresponding TOF values, (F) the ECSA slopes and (G) the current density normalized by ECSA for H_2Pc-COF (black curve), 0.25NiPc-COF (pink curve),

0.5NiPc-COF (red curve), 0.75NiPc-COF (blue curve), NiPc-COF (green curve) from –0.5 to –1.0 V in 0.5 M $KHCO_3$ under CO_2 atmosphere.

To further investigate the CO_2RR performance of the XNiPc-COFs, using a H-cell separated by a Nafion-117 membrane in the 0.5 M $KHCO_3$ solution with a three-electrode configuration under the saturated CO_2. The linear sweep voltammetry curves (LSV) demonstrated that these XNiPc-COFs had a small onset potential (Figure 4A). The kinetic behaviours for synthesized COFs were revealed by Tafel slopes (Figure 4B). And the Tafel slope of the 0.5NiPc-COF, 0.75NiPc-COF were 134 and 123 mV dec^{-1}, which much lower than that of H_2Pc-COF, 0.25NiPc-COF and NiPc-COF with values of 340, 364 and 182 mV dec^{-1}, respectively, indicating that the formation of *COOH from the adsorbed CO_2 via a proton-coupled electron transfer process is the rate determining step (RDS) for the 0.5NiPc-COF and 0.75NiPc-COF.[53] However, the much higher Tafel slopes of H_2Pc-COF, 0.25NiPc-COF and NiPc-COF suggested the slow kinetic process.

To explore the selectivity of COFs for CO_2RR, the gas products at different applied potentials from –0.5 to –1.0 V for 300 s were analysed (Figure S31). It showed CO and H_2 were observed and no liquid product was produced in the CO_2RR process. The Faradaic efficiencies of CO (FE_{CO}) for the H_2Pc-COF were 23.12%, 27.41%, 32.56%, 34.21%, 29.88% and 26.18% from –0.5 to –1.0 V, respectively (Figure 4C, black curve). The FE_{CO} of the conductive carbon were 2.22%, 3.12%, 6.13%, 9.25%, 3.34% and 4.02% at –0.5, –0.6, –0.7, –0.8, –0.9 and –1.0 V, respectively, suggesting its little contribution of CO_2RR performance (Figure S32). In addition, we calculated the partial CO current density (j_{CO}) to evaluate the activity. The H_2Pc-COF demonstrated the maximum j_{CO} of 3.91 mA cm^{-2} at –1.0 V. The selectivity was highly improved with the increasement of Ni-N sites of the structure, suggesting that H_2Pc units were not the active origin for CO_2RR (Table S4).

Although 0.25NiPc-COF has delivered more positive E_O, the selectivity and activity for CO products are still limited. And the maximum FE_{CO} was 37.66% at –0.8 V with a highest J_{co} of 6.34 mA cm^{-2} at –1.0 V, suggesting the more H_2Pc units in the frameworks caused H_2 as the major products. When the ratio between the H_2Pc and NiPc were 1/1 in 0.5NiPc-COF, the activity and selectivity for producing CO showed obvious enhanced (the maximum FE_{CO} was 92.52% at –0.8 V with a highest J_{co} of 25.08 mA cm^{-2} at –1.0 V) (Figure 4D, red curve). The 0.75NiPc-COF had higher selectivity than that of other XNiPc-COF in the same potential range, with FE_{CO} of 82.19%, 86.62%, 90.22%, 95.37%, 92.77%, and 88.54%, respectively (Figure 4C, blue curve). The highest j_{CO} was 25.50 mA cm^{-2} at –1.0 V, which was close to that of the 0.5NiPc-COFs, (Figure 4D, blue curve). The FE_{CO} for the NiPc-COF were 65.97%, 69.32%, 73.12%, 75.68%, 73.17%, and 67.21% at the same potentials (Figure 4C, red curve), and the highest j_{CO} was 16.17 mA cm^{-2} at a potential of –1.0 V, which was much lower than that of 0.5NiPc-COF and 0.75NiPc-COF (Figure 4D, green curve). These results further indicated that the alternate structure of H_2Pc and NiPc can improve the CO selectivity due to the H_2Pc units adjusted the local electron density of the active Ni-N sites, further improving the CO_2RR. We also tested the CO_2RR performance of 0.5NiPc-COF in the acidic aqueous solution under CO_2-atmosphere. Specifically, the FE_{CO} of the 0.5NiPc-COF were 19.43%, 21.02%, 22.11%, 20.43%, 19.31% and 17.52% at –0.3, –0.4, –0.5, –0.6, –0.7 and –0.8 V, respectively, indicating the lower activity in acidic solutions (Figure S33). The turnover frequencies (TOFs) of these XNiPc-COFs were calculated in the potential range of –0.5 to –1.0 V based on the loading of Ni-N sites in the XNiPc-COFs and N sites in the H_2Pc-COF as the catalytic origin. The calculated TOF values for the H_2Pc-COF, 0.25NiPc-COF, 0.5NiPc-COF, 0.75NiPc-COF and NiPc-COF were 1258.64, 2790.41, 4713.53, 3749.88 and 3860.12 h^{-1} at –1.0 V, respectively (Figure 4E). Thus, the alternate structure of H_2Pc and NiPc with the ratio of 1/1 for

the 0.5NiPc-COF, which possessed high utilization efficiency of Ni-N sites, facilitated both its activity and selectivity.

Giving that the different catalytic behaviours of the XNiPc-COFs, the electrochemical active surface areas (ECSAs) were measured. Specifically, the electrochemical double layer capacitances (C_{dl}) were obtained using cyclic voltammogram (CV) plots (Figure S34). The C_{dl} values for the H_2Pc-COF, 0.25NiPc-COF, 0.5NiPc-COF, 0.75NiPc-COF and NiPc-COF were 18.21, 17.89, 21.61, 25.06, and 18.76 mF cm^{-2}, respectively (Figure 4F). And the ECSA were then calculated by ECSA = C_{dl}/C_s, in which the C_s is 0.04 mF cm^{-2}.[54-57] Therefore, the evaluated ECSA for H_2Pc-COF, 0.25NiPc-COF, 0.5NiPc-COF, 0.75NiPc-COF and NiPc-COF were 455.25, 447.25, 540.25, 626.50 and 469. To investigate the different surface catalytic activity, we have normalized the J_{co} by ECSA, and the corresponding current density for the catalytic COFs at different potentials were in the order of 0.5NiPc-COF >0.75NiPc-COF > NiPc-COF >0.25NiPc-COF > H_2Pc-COF at diferent potentials, which further confirming the highest activity for 0.5NiPc-COF (Figure 4G).[58]

Furthermore, electrochemical impedance spectroscopy (EIS) was investigated. Nyquist plots and corresponding parameters showed that with the increasement of Ni-N sites, the 0.25NiPc-COF (61.18 Ω), 0.5NiPc-COF (33.27 Ω), 0.75NiPc-COF (59.71 Ω) and NiPc-COF (58.31 Ω). Specifically, they exhibited lower charge transfer resistance than that of the H_2Pc-COF (101.33 Ω), indicating that they were capable of faster electron transfer (Figure S35 and Table S5). In addition, the H_2Pc-COF showed the lowest diffusive resistance (3.32 Ω) compared with 0.25NiPc-COF (3.82 Ω), 0.5NiPc-COF (6.27 Ω), 0.75NiPc-COF (6.12 Ω) and NiPc-COF (7.02 Ω), revealing that the H_2Pc could ensure faster electron transfer from the electrodes to CO_2.

The long-term stability of the 0.5NiPc-COF was investigated at –0.8 V in CO_2-saturated $KHCO_3$ for 24 h (Figure S36). Specifically, a slight attenuation of FE_{CO} from 95.37% to 90.68% with a steady current density of 13.6 mA cm^{-2}, indicating the excellent long-term stability. After the long-term stability measurement, the PXRD patterns and FT IR and XPS spectra were obtained to confirm the structure. Specifically, the PXRD patterns revealed no obvious change of these peaks, indicating the maintenance of the structure. (Figure S37). Meanwhile, after the durability test, the Ni 2p and N 1s peaks observed, corresponding to are in good agreement with those found for fresh 0.5NiPc-COF (Figures S38-S39). Furthermore, the FT IR spectra disclose the lack of any significant band change between fresh 0.5NiPc-COF and used catalyst (Figure S40). These results demonstrated their remarkable durability of these XNiPc-COFs in electrocatalysis CO_2RR process.

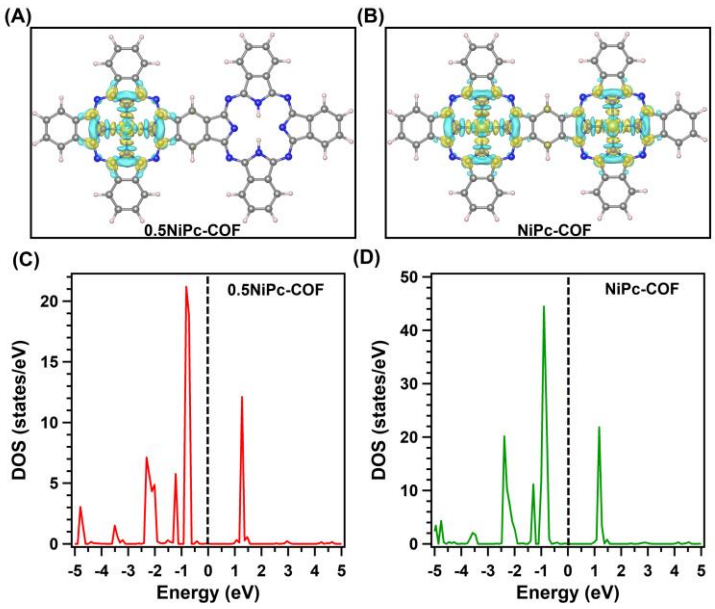

Figure 5. The electron density difference of (A) 0.5NiPc-COF and (B) NiPc-COF (The yellow and blue areas represent a gain and loss of electrons, respectively.).The projected density of states (pDOS) plots of (C) 0.5NiPc-COF and (D) NiPc-COF.

Density Functional Theory (DFT) calculations were adopted to further explain why 0.5NiPc-COF provides a better CO_2RR performance than NiPc-COF. Based on the experimental results, Ni-N was considered to be the active site for the CO_2RR, and 0.5NiPc-COF with a ratio of H_2Pc and NiPc of 1:1 and NiPc-COF structure models were constructed. the charge density difference of 0.5NiPc-COF clearly revealed that the Ni-N sites lost electrons (0.949 e^-) when the intermediates adsorption, while the NiPc-COF lost 1.062 e^- in this process, indicating the alternate structure of H_2Pc and NiPc could weaken the CO_2RR energy barrier (Figure 5A and 5B). The H_2Pc unites donated their electrons to NiPc units in the frameworks, and enhance the electron density of Ni sites with greater nucleophilicity and a stronger bond with Lewis acidic CO_2 molecules. In addition, the projected density of states (pDOS) plots were obtained for 0.5NiPc-COF and NiPc-COF (Figure 5C and 5D). The d band of the Ni-N site of 0.5NiPc-COF accommodates more electrons than that of NiPc-COF, further confirming that the electrons from H_2Pc are successfully transferred to NiPc. Furthermore, we used DFT to calculate the electron static potential (ESP) diagram of NiPc-COF and 0.5NiPc-COF. Specifically, ESP diagrams of NiPc-COF and 0.5NiPc-COF model revealed that the H_2Pc units can regulate the charge distribution. The electron-rich region (negative potential) of 0.5NiPc-COF is mainly distributed around the whole skeleton, while the pyridinic nitrogen of the NiPc-COF is more electron rich, indicating the formation of an internal electric field further promoting the CO_2RR of 0.5NiPc-COF (Figure S41). Additionally, the multiple components of H_2Pc and NiPc in the 0.5NiPc-COF can modulate the dipole moment. Specifically, the 0.5NiPc-COF (0.12 Debye) inhibits charge recombination and promotes charge transfer, resulting in a higher local charge redistribution than H_2Pc-COF (0.0006 Debye) and NiPc-COF (0 Debye) (Figure S42).[59-61]

Conclusion

In this study, a skeleton engineering strategy based on the multiple-component synthesis to construct the controllable metal density in the skeletons was first reported, which build the quantitative correlation between the metal density and catalytic performance. By establishing COFs with of vacancies and Ni-N sites, the 0.5NiPc-COF catalyzed CO_2RR with high selectivity and activity (FE_{CO} of 95.37% at –0.8 V and TOF of 4713.53 h^{-1} at –1.0 V). The design and modulation density of catalytic sites in COFs proposed not only new insights into electrocatalysis or energy conversion, but also guidance of constructing COFs with alternate structures of vacancies and metal sites for achieving high catalytic performance.

ASSOCIATED CONTENT

Supporting Information. Descriptions of characterization equipment and instrument. Synthesis methods of H_2Pc-COF, 0.25NiPc-COF, 0.5NiPc-COF, 0.75NiPc-COF and NiPc-COF. Electrocatalysis CO_2RR performance tests. Mott-Schottky curve test. The calculation methods of FE_{CO} and TOF values. XAFS measurements and data processing. The Staggered-AB model of H_2Pc-COF, 0.25NiPc-COF, 0.5NiPc-COF, 0.75NiPc-COF and NiPc-COF. Figures of FT IR, N_2 adsorption–desorption isotherms, UV-Vis spectra, Tauc plots, SEM, TEM, EDX-mapping images, chemical stability test, thermogravimetric curves, water contact angles, the XPS spectra of N 1s in-situ the CO_2 adsorption under the moderate pressure for H_2Pc-COF, 0.25NiPc-COF, 0.5NiPc-COF, 0.75NiPc-COF and NiPc-COF. The XANES spectra for Ni of Ni foil NiO. EXAFS fitting curves for Ni in NiPc, 0.25NiPc-COF, 0.5NiPc-COF, 0.75NiPc-COF and NiPc-COF. The LSV curves in N_2 atmosphere, the CV curves from 10 mV s^{-1} to 50 mV s^{-1}, Nyquist plots of H_2Pc-COF, 0.25NiPc-COF, 0.5NiPc-COF, 0.75NiPc-COF and NiPc-COF. Chronoamperometry test for CO_2RR, PXRD, FT IR spectra, XPS of N 1s, Ni 2p for 0.5NiPc-COF. The dipole moment calculation of H_2Pc-COF 0.5NiPc-COF and NiPc-COF.

AUTHOR INFORMATION

Corresponding Author

*Jun He: jun.he@nottingham.edu.cn

*Qing Xu: xuqing@sari.ac.cn

*Gaofeng Zeng: zenggf@sari.ac.cn

Author Contributions

Q. Xu. conceived the idea and designed the experiments. M. Liu. performed the experiments. Y. Fu. contributed to the theory calculation part. S. Yang performed the EXAFS experiments. M. Liu, Q. Xu. and G. Zeng. wrote and revised the manuscript. All the authors contributed to the data interpretation, discussion, and manuscript revision. All authors have given approval to the final version of the manuscript. & M. Liu. X. Zhao and S. Yang. contributed equally to this work.

NOTES

The authors declare no competing financial interest.

ACKNOWLEDGMENT

The authors acknowledge the financial supports from the National Natural Science Foundation of China (52303288, 21878322, 22075309, 22378413), the Science and Technology Commission of Shanghai Municipality (20ZR1464000, 22ZR1470100), the Youth Innovation Promotion Association of Chinese Academy of Sciences, and Biomaterials and Regenerative Medicine Institute Cooperative Research Project Shanghai Jiao Tong University School of Medicine (2022LHA09).

REFERENCES

(1) Nitopi, S.; Bertheussen, E.; Scott, S. B.; Liu, X.; Engstfeld, A. K.; Horch, S.; Seger, B.; Stephens, I. E. L.; Chan, K.; Hahn, C.; Nørskov, J. K.; Jaramillo, T. F.; Chorkendorff, I., Progress and Perspectives of Electrochemical CO_2 Reduction on Copper in Aqueous Electrolyte. *Chem. Rev.* **2019**, *119*, 7610-7672.

(2) Wu, Q. J.; Si, D. H.; Wu, Q.; Dong, Y. L.; Cao, R.; Huang, Y. B., Boosting Electroreduction of CO_2 over Cationic Covalent Organic Frameworks: Hydrogen Bonding Effects of Halogen Ions. *Angew. Chem. Int. Ed.* **2023**, *62*, e202215687.

(3) Han, B.; Ding, X.; Yu, B.; Wu, H.; Zhou, W.; Liu, W.; Wei, C.; Chen, B.; Qi, D.; Wang, H.; Wang, K.; Chen, Y.; Chen, B.; Jiang, J., Two-Dimensional Covalent Organic Frameworks with Cobalt(II)-Phthalocyanine Sites for Efficient Electrocatalytic Carbon Dioxide Reduction. *J. Am. Chem. Soc.* **2021**, *143*, 7104-7113.

(4) Han, B.; Jin, Y.; Chen, B.; Zhou, W.; Yu, B.; Wei, C.; Wang, H.; Wang, K.; Chen, Y.; Chen, B.; Jiang, J., Maximizing Electroactive Sites in a Three-Dimensional Covalent Organic Framework for Significantly Improved Carbon Dioxide Reduction Electrocatalysis. *Angew. Chem. Int. Ed.* **2022**, *61*, e202114244.

(5) Zhu, H.-J.; Lu, M.; Wang, Y.-R.; Yao, S.-J.; Zhang, M.; Kan, Y.-H.; Liu, J.; Chen, Y.; Li, S.-L.; Lan, Y.-Q., Efficient electron transmission in covalent organic framework nanosheets for highly active electrocatalytic carbon dioxide reduction. *Nat. Commun.* **2020**, *11*, 497.

(6) Liang, Z.; Wang, H.-Y.; Zheng, H.; Zhang, W.; Cao, R., Porphyrin-based frameworks for oxygen electrocatalysis and catalytic reduction of carbon dioxide. *Chem. Soc. Rev.* **2021,** *50* (4), 2540-2581.

(7) Liu, M.; Yang, S.; Yang, X.; Cui, C.-X.; Liu, G.; Li, X.; He, J.; Chen, G. Z.; Xu, Q.; Zeng, G., Post-synthetic modification of covalent organic frameworks for CO_2 electroreduction. *Nat. Commun.* **2023,** *14*, 3800.

(8) Askins, E. J.; Zoric, M. R.; Li, M.; Luo, Z.; Amine, K.; Glusac, K. D., Toward a mechanistic understanding of electrocatalytic nanocarbon. *Nat Commun.* **2021,** *12*, 3288.

(9) Qiu, X.-F.; Huang, J.-R.; Yu, C.; Zhao, Z.-H.; Zhu, H.-L.; Ke, Z.; Liao, P.-Q.; Chen, X.-M., A Stable and Conductive Covalent Organic Framework with Isolated Active Sites for Highly Selective Electroreduction of Carbon Dioxide to Acetate. *Angew. Chem. Int. Ed.* **2022,** *61*, e202206470.

(10) Gong, Y.-N.; Zhong, W.; Li, Y.; Qiu, Y.; Zheng, L.; Jiang, J.; Jiang, H.-L., Regulating Photocatalysis by Spin-State Manipulation of Cobalt in Covalent Organic Frameworks. *J. Am. Chem. Soc.* **2020,** *142*, 16723-16731.

(11) Zhou, J.; Li, J.; Kan, L.; Zhang, L.; Huang, Q.; Yan, Y.; Chen, Y.; Liu, J.; Li, S.-L.; Lan, Y.-Q., Linking oxidative and reductive clusters to prepare crystalline porous catalysts for photocatalytic CO_2 reduction with H_2O. *Nat. Commun.* **2022,** *13*, 4681.

(12) Liu, H.; Chu, J.; Yin, Z.; Cai, X.; Zhuang, L.; Deng, H., Covalent Organic Frameworks Linked by Amine Bonding for Concerted Electrochemical Reduction of CO_2. *Chem* **2018**, *4*, 1696-1709.

(13) Zhang, M.-D.; Si, D.-H.; Yi, J.-D.; Zhao, S.-S.; Huang, Y.-B.; Cao, R., Conductive Phthalocyanine-Based Covalent Organic Framework for Highly Efficient Electroreduction of Carbon Dioxide. *Small* **2020**, *16*, 2005254.

(14) Wu, Q.; Mao, M.-J.; Wu, Q.-J.; Liang, J.; Huang, Y.-B.; Cao, R., Construction of Donor–Acceptor Heterojunctions in Covalent Organic Framework for Enhanced CO_2 Electroreduction. *Small* **2021**, *17*, 2004933.

(15) Yan, X.; Lyu, S.; Xu, X.-Q.; Chen, W.; Shang, P.; Yang, Z.; Zhang, G.; Chen, W.; Wang, Y.; Chen, L., Superhydrophilic 2D Covalent Organic Frameworks as Broadband Absorbers for Efficient Solar Steam Generation. *Angew. Chem. Int. Ed.* **2022**, *61*, e202201900.

(16) Zou, L.; Sa, R.; Zhong, H.; Lv, H.; Wang, X.; Wang, R., Photoelectron Transfer Mediated by the Interfacial Electron Effects for Boosting Visible-Light-Driven CO_2 Reduction. *ACS Catal.* **2022**, *12*, 3550-3557.

(17) Wu, Q.-J.; Liang, J.; Huang, Y.-B.; Cao, R., Thermo-, Electro-, and Photocatalytic CO_2 Conversion to Value-Added Products over Porous Metal/Covalent Organic Frameworks. *Acc. Chem. Res.* **2022**, *55*, 2978-2997.

(18) Han, B.; Ding, X.; Yu, B.; Wu, H.; Zhou, W.; Liu, W.; Wei, C.; Chen, B.; Qi, D.; Wang, H.; Wang, K.; Chen, Y.; Chen, B.; Jiang, J., Two-Dimensional Covalent Organic Frameworks with Cobalt(II)-Phthalocyanine Sites for Efficient Electrocatalytic Carbon Dioxide Reduction. *J. Am. Chem. Soc.* **2021**, *143*, 7104-7113.

(19) Chi, S.-Y.; Chen, Q.; Zhao, S.-S.; Si, D.-H.; Wu, Q.-J.; Huang, Y.-B.; Cao, R., Three-dimensional porphyrinic covalent organic frameworks for highly efficient electroreduction of carbon dioxide. *J. Mater. Chem. A* **2022**, *10*, 4653-4659.

(20) Zhou, T.; Wang, L.; Huang, X.; Unruangsri, J.; Zhang, H.; Wang, R.; Song, Q.; Yang, Q.; Li, W.; Wang, C.; Takahashi, K.; Xu, H.; Guo, J., PEG-stabilized coaxial stacking of two-dimensional covalent organic frameworks for enhanced photocatalytic hydrogen evolution. *Nat. Commun.* **2021**, *12*, 3934.

(21) Wang, Y.-R.; Ding, H.-M.; Ma, X.-Y.; Liu, M.; Yang, Y.-L.; Chen, Y.; Li, S.-L.; Lan, Y.-Q., Imparting CO_2 Electroreduction Auxiliary for Integrated Morphology Tuning and Performance Boosting in a Porphyrin-based Covalent Organic Framework. *Angew. Chem. Int. Ed.* **2022**, *61*, e202114648.

(22) Wu, Z.; Wu, H.; Cai, W.; Wen, Z.; Jia, B.; Wang, L.; Jin, W.; Ma, T., Engineering Bismuth–Tin Interface in Bimetallic Aerogel with a 3D Porous Structure for Highly Selective Electrocatalytic CO_2 Reduction to HCOOH. *Angew. Chem. Int. Ed.* **2021**, *60*, 12554-12559.

(23) Li, Z.; Sheng, L.; Hsueh, C.; Wang, X.; Cui, H.; Gao, H.; Wu, Y.; Wang, J.; Tang, Y.; Xu, H.; He, X., Three-Dimensional Covalent Organic Frameworks with hea Topology. *Chem. Mater.* **2021**, *33*, 9618-9623.

(24) Wang, L.; Zeng, C.; Xu, H.; Yin, P.; Chen, D.; Deng, J.; Li, M.; Zheng, N.; Gu, C.; Ma, Y., A highly soluble, crystalline covalent organic framework compatible with device implementation. *Chem. Sci.* **2019**, *10*, 1023-1028.

(25) Yue, Y.; Li, H.; Chen, H.; Huang, N., Piperazine-Linked Covalent Organic Frameworks with High Electrical Conductivity. *J. Am. Chem. Soc.* **2022**, *144*, 2873-2878.

(26) Chen, X.; Li, Y.; Wang, L.; Xu, Y.; Nie, A.; Li, Q.; Wu, F.; Sun, W.; Zhang, X.; Vajtai, R.; Ajayan, P. M.; Chen, L.; Wang, Y., High-Lithium-Affinity Chemically Exfoliated 2D Covalent Organic Frameworks. *Adv. Mater.* **2019**, *31*, 1901640.

(27) Kou, M.; Wang, Y.; Xu, Y.; Ye, L.; Huang, Y.; Jia, B.; Li, H.; Ren, J.; Deng, Y.; Chen, J.; Zhou, Y.; Lei, K.; Wang, L.; Liu, W.; Huang, H.; Ma, T., Molecularly Engineered Covalent Organic Frameworks for Hydrogen Peroxide Photosynthesis. *Angew. Chem. Int. Ed.* **2022**, *61*, e202200413.

(28) Liu, M.; Kong, H.-Y.; Bi, S.; Ding, X.; Chen, G. Z.; He, J.; Xu, Q.; Han, B.-H.; Zeng, G., Non-Interpenetrated 3D Covalent Organic Framework with Dia Topology for Au Ions Capture. *Adv. Funct. Mater.* **2023**, 2302637, DOI: 10.1002/adfm.202302637.

(29) Su, Y.; Wan, Y.; Xu, H.; Otake, K.-i.; Tang, X.; Huang, L.; Kitagawa, S.; Gu, C., Crystalline and Stable Benzofuran-Linked Covalent Organic Frameworks from Irreversible Cascade Reactions. *J. Am. Chem. Soc.* **2020**, *142*, 13316-13321.

(30) Wang, L.; Xu, C.; Zhang, W.; Zhang, Q.; Zhao, M.; Zeng, C.; Jiang, Q.; Gu, C.; Ma, Y., Electrocleavage Synthesis of Solution-Processed, Imine-Linked, and Crystalline Covalent Organic Framework Thin Films. *J. Am. Chem. Soc.* **2022**, *144*, 8961-8968.

(31) Yang, Z.; Liu, J.; Li, Y.; Zhang, G.; Xing, G.; Chen, L., Arylamine-Linked 2D Covalent Organic Frameworks for Efficient Pseudocapacitive Energy Storage. *Angew. Chem. Int. Ed.* **2021**, *60*, 20754-20759.

(32) Chen, W.; Wang, L.; Mo, D.; He, F.; Wen, Z.; Wu, X.; Xu, H.; Chen, L., Modulating Benzothiadiazole-Based Covalent Organic Frameworks via Halogenation for Enhanced Photocatalytic Water Splitting. *Angew. Chem. Int. Ed.* **2020**, *59*, 16902-16909.

(33) He, C.; Si, D. H.; Huang, Y. B.; Cao, R., A CO_2-Masked Carbene Functionalized Covalent Organic Framework for Highly Efficient Carbon Dioxide Conversion. *Angew. Chem. Int. Ed.* **2022**, *61*, e202207478.

(34) Wang, S.; Yang, L.; Xu, K.; Chen, H.; Huang, N., De Novo Fabrication of Large-Area and Self-Standing Covalent Organic Framework Films for Efficient Separation. *ACS Appl. Mater. Interfaces* **2021**, *13*, 44806-44813.

(35) Liu, M.; Liu, S.; Cui, C. X.; Miao, Q.; He, Y.; Li, X.; Xu, Q.; Zeng, G., Construction of Catalytic Covalent Organic Frameworks with Redox-Active Sites for the Oxygen Reduction and the Oxygen Evolution Reaction. *Angew. Chem. Int. Ed.* **2022**, *61*, e202213522.

(36) Guo, C.; Zhou, J.; Chen, Y.; Zhuang, H.; Li, Q.; Li, J.; Tian, X.; Zhang, Y.; Yao, X.; Chen, Y.; Li, S. L.; Lan, Y. Q., Synergistic Manipulation of Hydrogen Evolution and Zinc Ion Flux in Metal-Covalent Organic Frameworks for Dendrite-free Zn-based Aqueous Batteries. *Angew. Chem. Int. Ed.* **2022**, *61*, e202210871.

(37) Zhao, X.; Pachfule, P.; Li, S.; Langenhahn, T.; Ye, M.; Schlesiger, C.; Praetz, S.; Schmidt, J.; Thomas, A., Macro/Microporous Covalent Organic Frameworks for Efficient Electrocatalysis. *J. Am. Chem. Soc.* **2019**, *141*, 6623-6630.

(38) Liu, M.; Yang, S.; Liu, S.; Miao, Q.; Yang, X.; Li, X.; Xu, Q.; Zeng, G., Construction of Atomic Metal-N_2 Sites by Interlayers of Covalent Organic Frameworks for Electrochemical H_2O_2 Synthesis. *Small* **2022**, *18*, e2204757.

(39) Lin, C. Y.; Zhang, D.; Zhao, Z.; Xia, Z., Covalent Organic Framework Electrocatalysts for Clean Energy Conversion. *Adv. Mater.* **2018**, *30*, 1703646.

(40) Lin, S.; Diercks, C. S.; Zhang, Y.-B.; Kornienko, N.; Nichols, E. M.; Zhao, Y.; Paris, A. R.; Kim, D.; Yang, P.; Yaghi, O. M.; Chang, C. J., Covalent organic frameworks comprising cobalt porphyrins for catalytic CO_2 reduction in water. *Science* **2015**, *349*, 1208-1213.

(41) Lu, M.; Liu, J.; Li, Q.; Zhang, M.; Liu, M.; Wang, J.-L.; Yuan, D.-Q.; Lan, Y.-Q., Rational Design of Crystalline Covalent Organic Frameworks for Efficient CO_2 Photoreduction with H_2O. *Angew. Chem. Int. Ed.* **2019**, *58*, 12392-12397.

(42) Lu, C.; Yang, J.; Wei, S.; Bi, S.; Xia, Y.; Chen, M.; Hou, Y.; Qiu, M.; Yuan, C.; Su, Y.; Zhang, F.; Liang, H.; Zhuang, X., Atomic Ni Anchored Covalent Triazine Framework as High Efficient Electrocatalyst for Carbon Dioxide Conversion. *Adv. Funct. Mater.* **2019**, *29*, 1806884.

(43) Li, Y.; Chen, Q.; Xu, T.; Xie, Z.; Liu, J.; Yu, X.; Ma, S.; Qin, T.; Chen, L., De Novo Design and Facile Synthesis of 2D Covalent Organic Frameworks: A Two-in-One Strategy. *J. Am. Chem. Soc.* **2019**, *141*, 13822-13828.

(44) Xu, X.; Cai, P.; Chen, H.; Zhou, H.-C.; Huang, N., Three-Dimensional Covalent Organic Frameworks with she Topology. *J. Am. Chem. Soc.* **2022**, *144*, 18511-18517.

(45) Xu, X.; Wu, X.; Xu, K.; Xu, H.; Chen, H.; Huang, N., Pore partition in two-dimensional covalent organic frameworks. *Nat. Commun.* **2023**, *14*, 3360.

(46) Su, Y.; Li, B.; Xu, H.; Lu, C.; Wang, S.; Chen, B.; Wang, Z.; Wang, W.; Otake, K.-i.; Kitagawa, S.; Huang, L.; Gu, C., Multi-Component Synthesis of a Buta-1,3-diene-Linked Covalent Organic Framework. *J. Am. Chem. Soc.* **2022**, *144*, 18218-18222.

(47) Li, X.; Xiang, Z., Identifying the impact of the covalent-bonded carbon matrix to FeN4 sites for acidic oxygen reduction. *Nat. Commun.* **2022**, *13*, 57.

(48) Tian, X.; Huang, X.; Shi, J.-W.; Zhou, J.; Guo, C.; Wang, R.; Wang, Y.-R.; Lu, M.; Li, Q.; Chen, Y.; Li, S.-L.; Lan, Y.-Q., Implanting Built-In Electric Field in Heterometallic Phthalocyanine Covalent Organic Frameworks for Light-Assisted CO_2 Electroreduction. *CCS Chem.* **2023**, 1-10.

(49) Wang, S.; Wang, Q.; Shao, P.; Han, Y.; Gao, X.; Ma, L.; Yuan, S.; Ma, X.; Zhou, J.; Feng, X.; Wang, B., Exfoliation of Covalent Organic Frameworks into Few-Layer Redox-Active Nanosheets as Cathode Materials for Lithium-Ion Batteries. *J. Am. Chem. Soc.* **2017**, *139*, 4258-4261.

(50) Geng, Q.; Wang, H.; Wang, J.; Hong, J.; Sun, W.; Wu, Y.; Wang, Y., Boosting the Capacity of Aqueous Li-Ion Capacitors via Pinpoint Surgery in Nanocoral-Like Covalent Organic Frameworks. *Small Methods* **2022**, *6*, 2200314.

(51) Zhang, X.; Zhang, Z.; Li, H.; Gao, R.; Xiao, M.; Zhu, J.; Feng, M.; Chen, Z., Insight Into Heterogeneous Electrocatalyst Design Understanding for the Reduction of Carbon Dioxide. *Adv. Energy Mater.* **2022**, *12*, 2201461.

(52) Shang, Y.; Ding, Y.; Zhang, P.; Wang, M.; Jia, Y.; Xu, Y.; Li, Y.; Fan, K.; Sun, L., Pyrrolic N or pyridinic N: The active center of N-doped carbon for CO_2 reduction. *Chin. J. Catal.* **2022**, *43*, 2405-2413.

(53) Wang, L.; Chen, W.; Zhang, D.; Du, Y.; Amal, R.; Qiao, S.; Wu, J.; Yin, Z., Surface strategies for catalytic CO_2 reduction: from two-dimensional materials to nanoclusters to single atoms. *Chem. Soc. Rev.* **2019**, *48*, 5310-5349.

(54) Voiry, D.; Chhowalla, M.; Gogotsi, Y.; Kotov, N. A.; Li, Y.; Penner, R. M.; Schaak, R. E.; Weiss, P. S., Best Practices for Reporting Electrocatalytic Performance of Nanomaterials. *ACS Nano* **2018**, *12*, 9635-9638.

(55) Cao, C.; Ma, D.-D.; Jia, J.; Xu, Q.; Wu, X.-T.; Zhu, Q.-L., Divergent Paths, Same Goal: A Pair-Electrosynthesis Tactic for Cost-Efficient and Exclusive Formate Production by Metal–Organic-Framework-Derived 2D Electrocatalysts. *Adv. Mater.* **2021**, *33*, 2008631.

(56) McCrory, C. C. L.; Jung, S.; Peters, J. C.; Jaramillo, T. F., Benchmarking Heterogeneous Electrocatalysts for the Oxygen Evolution Reaction. *J. Am. Chem. Soc.* **2013**, *135*, 16977-16987.

(57) Sun, X.; Shao, Q.; Pi, Y.; Guo, J.; Huang, X., A general approach to synthesise ultrathin NiM (M = Fe, Co, Mn) hydroxide nanosheets as high-performance low-cost electrocatalysts for overall water splitting. *J. Mater. Chem. A* **2017**, *5*, 7769-7775.

(58) Li, N.; Si, D.-H.; Wu, Q.-j.; Wu, Q.; Huang, Y.-B.; Cao, R., Boosting Electrocatalytic CO_2 Reduction with Conjugated Bimetallic Co/Zn Polyphthalocyanine Frameworks. *CCS Chem.* **2022**, *0*, 1-14.

(59) Carsten, B.; Szarko, J. M.; Son, H. J.; Wang, W.; Lu, L.; He, F.; Rolczynski, B. S.; Lou, S. J.; Chen, L. X.; Yu, L., Examining the Effect of the Dipole Moment on Charge Separation in Donor–Acceptor Polymers for Organic Photovoltaic Applications. *J. Am. Chem. Soc.* **2011**, *133*, 20468-20475.

(60) Wu, C.; Teng, Z.; Yang, C.; Chen, F.; Yang, H. B.; Wang, L.; Xu, H.; Liu, B.; Zheng, G.; Han, Q., Polarization Engineering of Covalent Triazine Frameworks for Highly Efficient Photosynthesis of Hydrogen Peroxide from Molecular Oxygen and Water. *Adv. Mater.* **2022**, *34*, 2110266.

(61) Yu, F.; Zhu, Z.; Wang, S.; Wang, J.; Xu, Z.; Song, F.; Dong, Z.; Zhang, Z., Novel donor-acceptor-acceptor ternary conjugated microporous polymers with boosting forward charge separation and suppressing backward charge recombination for photocatalytic reduction of uranium (VI). *Appl. Catal. B* **2022**, *301*, 120819.

Table of Contents